Original Article

Associations between tumor grade, contrast-enhanced ultrasound features, and microvascular density in patients with clear cell renal cell carcinoma: a retrospective study

Xia Meng, Ran Yang, Shengnan Zhao, Zhixia Sun, Hui Wang

China-Japan Union Hospital of Jilin University, Changchun, China

Contributions: (I) Conception and design: Z Sun, H Wang, X Meng; (II) Administrative support: Z Sun, H Wang; (III) Provision of study materials and patients: Z Sun, H Wang; (IV) Collection and assembly of data: X Meng, R Yang, S Zhao; (V) Data analysis and interpretation: X Meng; (VI) Manuscript writing: All authors; (VII) Final approval: All authors.

Correspondence to: Zhixia Sun; Hui Wang. China-Japan Union Hospital of Jilin University, Changchun 130033, China.
Email: sunzx@jlu.edu.cn; whui66@jlu.edu.cn.

Background: Clear cell renal cell carcinoma (ccRCC) comprises 70% of all renal cell carcinomas (RCCs). Currently, the most important prognostic factor for this type of carcinoma is the World Health Organization/International Society of Urological Pathology (WHO/ISUP) grade. However, nonsurgical methods are rarely used to determine a tumor's WHO/ISUP grade, thus limiting the development of nonsurgical therapies. Due to variations in microvascular density (MVD) at different stages of tumor growth, contrast-enhanced ultrasound (CEUS) features may provide a noninvasive method for evaluating the WHO/ISUP grade of ccRCC.

Methods: In this study, we analyzed confirmed cases of ccRCC using CEUS features. We also used CD34 and CD31 antibodies to determine MVD. The heterogeneity of CD34 and CD31 expressions were used to determine different degrees of angiogenesis.

Results: When compared to WHO/ISUP grade I/II (G1/G2) tumors, grade III/IV (G3/G4) tumors had reduced peak intensity (PI) (P=0.006), time to peak (TTP) (P<0.001), and relative enhancement percentage index (ΔPI%) (P<0.001). However, the frequency of incomplete pseudocapsule (P=0.049) and slow wash-in (P=0.001) was significantly higher in G3/G4 tumors. A cut-off value of ΔPI% <33.15% (P<0.001) allowed identification of G3/G4 tumors with an area under the curve (AUC) of 0.80 [95% confidence interval (CI): 0.70 to 0.91) and a sensitivity of 80%. The mean CD34$^+$ MVD (P<0.001) and CD31$^+$ MVD (P<0.001) were significantly lower in G3/G4 tumors. A positive correlation was revealed between ΔPI% and MVD. There was a statistically significant difference in the density of undifferentiated vessels between the slow wash-in and fast wash-in cases (P<0.001).

Conclusions: The features of CEUS are effective for differentiating G3/G4 tumors from G1/G2. There was a positive correlation detected between ΔPI% and MVD, and the density of undifferentiated vessels showed a significant difference between slow wash-in and fast wash-in cases. These findings indicate that CEUS can enable the sonographic visualization of tumor angiogenesis and thus be considered an acceptable method for the nonsurgical assessment of tumor microvascular distribution and grade.

Keywords: Clear cell renal cell carcinoma (ccRCC); contrast-enhanced ultrasound (CEUS); microvascular density (MVD)

Introduction

Renal cell carcinomas (RCCs) account for 90% of all renal cancers, and 70% of RCC are clear cell RCCs (ccRCC), which is the most aggressive subtype (1). Surgical treatment remains the main clinical therapy for ccRCC (2), but even when renal tumor resection is carried out during the early stages of tumor development, 20–30% of patients still develop local or distal metastases (3). Furthermore, within 3–5 years after radical nephrectomy, the likelihood of developing chronic kidney disease is still 30–50%, and patient quality of life remains poor (4). For this reason, nonsurgical treatment methods (5) are important for improving the survival rate and quality of life of patients with renal tumors.

The most reliable independent prognostic factor for assessing ccRCC remission is the World Health Organization/International Society of Urological Pathology (WHO/ISUP) grade (6). However, at present, the lack of available nonsurgical methods to evaluate the WHO/ISUP grade limits the clinical application and prognostic assessment of nonsurgical treatments.

Angiogenesis plays a crucial role in the growth and metastasis of most human tumors (7). The malignancy of ccRCC is a highly vascularized, and studies have shown that the expression of vascular endothelial growth factor (VEGF) in ccRCC is 5 times that of other renal cancer subtypes. An evaluation of the angiogenesis of solid tumors can be carried out by assessing microvascular density (MVD), which is an independent prognostic factor (8). However, ccRCC angiogenesis is complex. Studies have shown that there are at least 2 types of blood vessels in tumor angiogenesis: differentiated and undifferentiated blood vessels. Tumors with a high density of the latter type have a poor prognosis (9). Currently, there is a lack of nonsurgical methods for MVD evaluation, and there are even fewer studies on the degree of tumor angiogenesis differentiation. Nevertheless, imaging enhancement of RCC is positively correlated with MVD (10). In some studies, contrast-enhanced ultrasound (CEUS) has been used to classify RCC histologic subtypes, and real-time CEUS has been found to be helpful for displaying the microvascular perfusion pattern of the lesion (11). In fact, CEUS features can be described by a contrast analysis software that can obtain its quantitative and qualitative parameters. Despite this, CEUS has never been used to study the tumor grade of ccRCCs (12,13). Therefore, in this *in vivo* study, we sought to determine the correlation between CEUS parameters, ccRCC MVD, degree of angiogenesis differentiation, and tumor grade to assess the efficacy and value of CEUS in evaluating tumor angiogenesis and grade.

Methods

Study population

This study was conducted in accordance with the Declaration of Helsinki (as revised in 2013) and was approved by the Ethics Committee of the China-Japan Union Hospital of Jilin University. Written informed consent was provided by all participants. We acquired 86 tumor specimens at our institution between January 2017 and September 2020 via partial or total nephrectomy. The inclusion criteria were a histopathological diagnosis of ccRCC and available preoperative CEUS imaging. The exclusion criterion was prior systemic therapy for metastatic disease. The clinicopathological characteristics of the participants are shown in *Table 1*. Histopathological analysis revealed low-grade (WHO/ISUP grade I/II) tumors in 56 cases and high-grade (WHO/ISUP grade III/IV) tumors in 30 cases. The flow chart for the patient selection process is shown in *Figure 1*.

CEUS examination and image analysis

Conventional ultrasound was used to select the best section of the tumor and adjacent renal cortex. The CEUS examinations were performed on the MyLab™ Twice (Esaote, Genova, Italy) and Resona 7 (Mindray Medical Inc., Shenzhen, China) ultrasound devices. The ultrasound contrast agent (25 mg; SonoVue, Bracco Imaging, Milan, Italy) was shaken for 15 s with 5 mL of 0.9% saline solution, and 1.2–1.6 mL of this suspension was injected as a bolus through the antecubital vein. We then injected 5 mL of 0.9% saline solution to quickly flush the bolus. To select the section with the lowest mechanical index (0.10) after initiation of CEUS imaging, the video system was started to record the whole course of the examination. In the process of imaging, the patient was asked to breathe smoothly so that the contrast agent wash-in and wash-out phases could be dynamically observed for 3–5 min. Then, QontraXt software (AMID, Rome, Italy) was started, and the whole process of CEUS was played back dynamically. The entire renal ultrasonogram was drawn first, and 2 regions of interest (ROIs), namely ROI1 and ROI2, were delineated. We selected ROI1 because it was the most obvious portion

Table 1 Baseline characteristics

Characteristics	Low grade (WHO/ISUP grade I and II)	High grade (WHO/ISUP grade III and IV)	P value
Gender			
Male	37	5	
Female	19	25	
Mean age (range), years	54 (25–79)	58 (39–74)	
Laterality of tumor			
Right kidney	30	14	
Left kidney	26	16	
Mean tumor size (range), cm	3.46 (1.5–8)	5.29 (2–13)	<0.05
WHO/ISUP grade			
I	11	0	
II	45	0	
III	0	25	
IV	0	5	
$CD34^+$ MVD	60.38 (±21.62)	30.99 (±11.85)	<0.001
$CD31^+$ MVD	68.41 (±21.91)	50.47 (±17.34)	<0.001
Undifferentiated vessels MVD	8.00 (±3.35)	19.47 (±9.76)	<0.001

WHO/ISUP, World Health Organization/International Society of Urological Pathology; MVD, microvascular density.
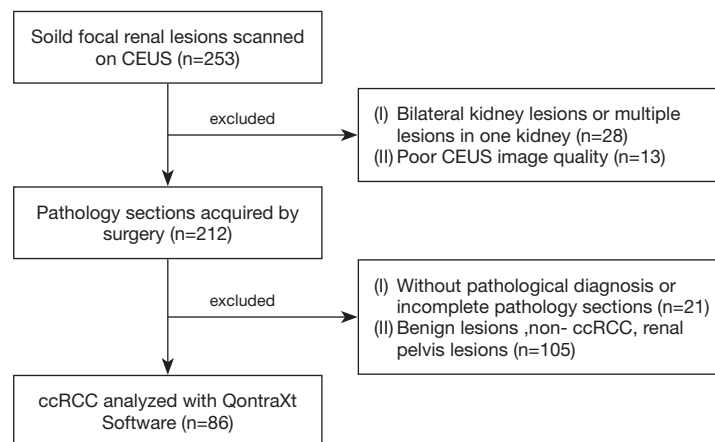
Figure 1 Flow chart of the patient selection process. CEUS, contrast-enhanced ultrasound; ccRCC, clear cell renal cell carcinoma.

after edge enhancement of the ccRCC tumor, whereas the normal renal cortex at the same depth adjacent to the tumor was defined as ROI2. These areas were deemed to be the most like each other. During the process of ROI delineation, enhancement-free areas, calcification, and the renal capsule were excluded. The placement of ROIs in the tumoral area and adjacent renal parenchyma is shown in *Figure 2*.

A time-intensity curve (TIC) was drawn, and its parameters were recorded. The quantitative parameters included peak intensity (PI), time to peak (TTP), and the relative enhancement percentage index (ΔPI%). The
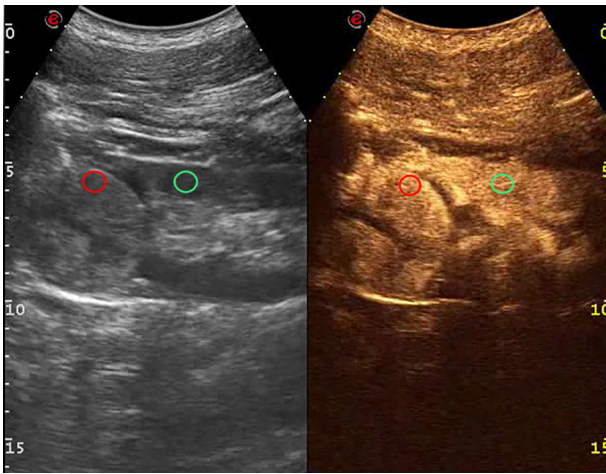
Figure 2 The placement of ROIs in the tumor (red circle) and adjacent renal parenchyma (green circle). ROIs, regions of interest.

$\Delta PI\%$ was calculated as follows: $\Delta PI\%=(Pt-Pc)/Pc100\%$, where Pt = peak of the tumor and Pc = peak of the adjacent renal cortex (14). Qualitative parameters included the speed of wash-in, the speed of wash-out, homogeneity of enhancement, and the integrity of the pseudocapsule. Slow wash-in was determined to have occurred when the TIC upward branch slope of the tumor was smaller or the same as that of the adjacent renal parenchyma. Slow wash-out was determined to have occurred when the TIC downward branch slope of the tumor was smaller or the same as that of the adjacent renal parenchyma. The pseudocapsule sign was defined as an enhanced rim of tumoral tissue. We enlisted 2 experts with more than 5 years of CEUS experience, who were blinded to patient information, including pathological diagnosis, to perform both CEUS and CEUS software evaluations.

MVD analysis and angiogenesis differentiation

From each of the 86 tumor specimens, 2 sections (4-μm thick) were prepared by paraffin wax embedding, and the histological sections were stained with hematoxylin and eosin. Mouse monoclonal anti-CD34 and anti-CD31 antibodies (Roche Corporation, Basel, Switzerland) were used to visualize the endothelial cells. The positivity of CD34 and CD31 was determined by brown-yellow staining on the surface of the tumor's vascular endothelial cell membrane, and MVD was quantified according to the Weidner method (15). Each specimen was observed under a low-power lens (×100), and a high density of

endothelial structures was chosen as the hotspot. The number of microvessels was counted in the 5 fields with the highest MVD under a high-power lens (×400), and the mean value was calculated. As each case was evaluated using the difference between 2 consecutive slides of CD31 and CD34 expression, the immunohistochemical staining quality was highly controlled and the hotspots were defined by the most vascularized areas of CD31 staining (16). In terms of expression location, CD34 is expressed in differentiated microvessels, while CD31 is expressed in both undifferentiated and differentiated microvessels. The expression heterogeneity of CD31 and CD34 in differentiated and undifferentiated vessels was used to obtain the count of undifferentiated microvessels by subtracting the CD34$^+$ vessel count from the CD31$^+$ vessel count (9,16). The processing and analysis of tissue specimens were performed by pathologists at our hospital who were blinded to the results of the CEUS findings.

Statistical analysis

The software SPSS 23.0 (IBM, Armonk, NY, USA) was used for statistical analysis. The qualitative data were expressed as frequencies, whereby normally distributed quantitative data were statistically described by mean ± standard deviation, and the data with skewed distribution were expressed through median and range. The chi-square test and independent samples t-test were used to compare the frequency and the mean of the 2 ROIs. A Wilcoxon signed-rank test was used for skewed data. A receiver operating characteristic (ROC) analysis was used to determine the optimal cut-off values for $\Delta PI\%$. Spearman rank correlation was used to evaluate the association between $\Delta PI\%$ and MVD. Statistical significance was set at P<0.05. All statistical analysis results are provided in *Tables 1,2*.

Results

Association between CEUS features and WHO/ISUP grade

Regarding the CEUS quantitative analysis of PI, $\Delta PI\%$, and TTP, there were significantly different values between high- and low-grade ccRCC tumors (P<0.05). We found that the PI and $\Delta PI\%$ were lower, and the TTP shorter, in high-grade ccRCC tumors (*Figures 3,4*). Among the qualitative parameters of CEUS, the frequency of a complete pseudocapsule and slow wash-in were significantly higher in high-grade ccRCC (P<0.05). High-grade tumors were also

1886

Meng et al. Contrast-enhanced ultrasound for ccRCC

Table 2 CEUS features of ccRCCs across different grades

Features	Low grade (WHO/ISUP grade I and II) (n=56)	High grade (WHO/ISUP grade III and IV) (n=30)	P value
TTP (range), s	76.00 (56.25–114.00)	21.00 (15.00–35.25)	<0.001
PI	42.01 (±12.41)	35.67 (±8.20)	0.006
ΔPI% (range), %	43.95 (38.28–62.95)	17.35 (7.78–32.40)	<0.001
Wash-in			0.001
Fast wash-in	41	11	
Slow wash-in	15	19	
Wash-out			0.353
Fast wash-out	32	14	
Slow wash-out	24	16	
Homogeneous			0.100
Present	23	7	
Absent	33	23	
Pseudocapsule			0.049
Complete	33	11	
Incomplete	23	19	

CEUS, contrast-enhanced ultrasound; ccRCCs, renal clear cell carcinomas; WHO/ISUP, World Health Organization/International Society of Urological Pathology; TTP, time to peak; PI, peak intensity; ΔPI%, relative enhancement percentage index.
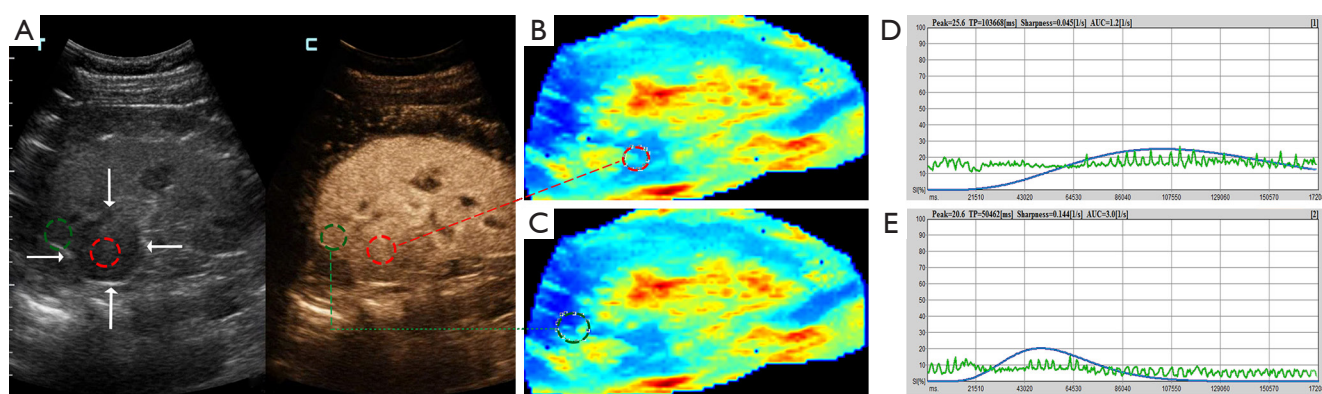

Figure 3 Ultrasound images of high-grade ccRCC in a 63-year-old woman. (A) Conventional ultrasound and CEUS images of the tumor; (B,C) chromatic maps with ROIs: (B) ROI1 for the analysis area and (C) ROI2 for the reference area; (D,E) intensity-time curves obtained using QontraXt software with PI, TTP, and ΔPI%. ccRCC, clear cell renal cell carcinoma; CEUS, contrast-enhanced ultrasound; ROIs, regions of interest; PI, peak intensity; TTP, time to peak; ΔPI%, relative enhancement percentage index.

characterized by a lack of blood supply. The wash-out speed and the homogeneity of enhancement were not significantly different between low- and high-grade tumors. The ROC analysis revealed that a cut-off value of ΔPI% <33.15% with an area under the curve (AUC) of 0.80 [95% confidence interval (CI): 0.70 to 0.91] allowed for the identification of high-grade tumors with a specificity of 82.1% and a sensitivity of 80% (*Figure 5*).
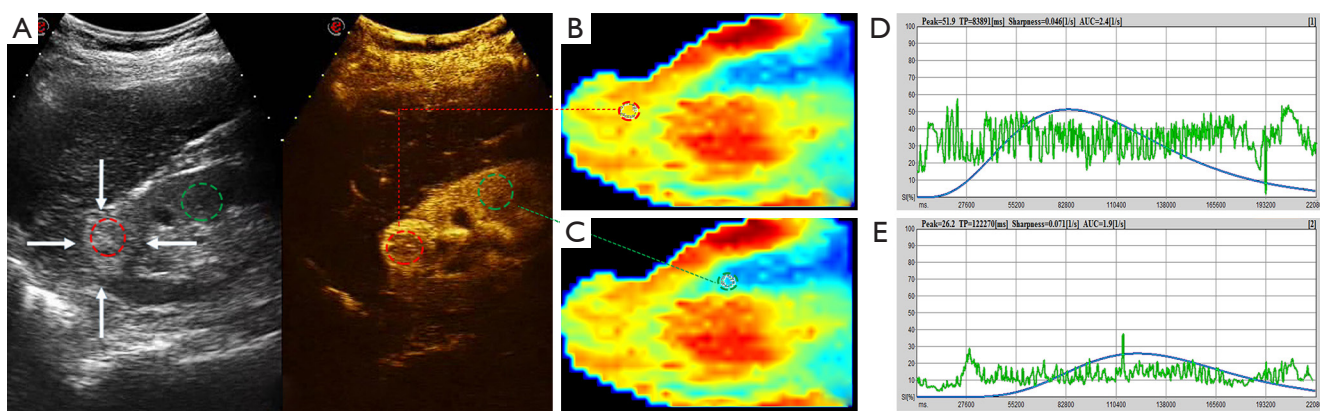
Figure 4 Ultrasound images of low-grade ccRCC in a 45-year-old man. (A) Conventional ultrasound and CEUS images of the tumor; (B,C) chromatic maps with ROIs: (B) ROI1 for the analysis area and (C) ROI2 for the reference area; (D,E) intensity-time curves obtained using QontraXt software with PI, TTP, and ΔPI%. ccRCC, clear cell renal clear cell carcinoma; CEUS, contrast-enhanced ultrasound; ROIs, region of interests; PI, peak intensity; TTP, time to peak; ΔPI%, relative enhancement percentage index.
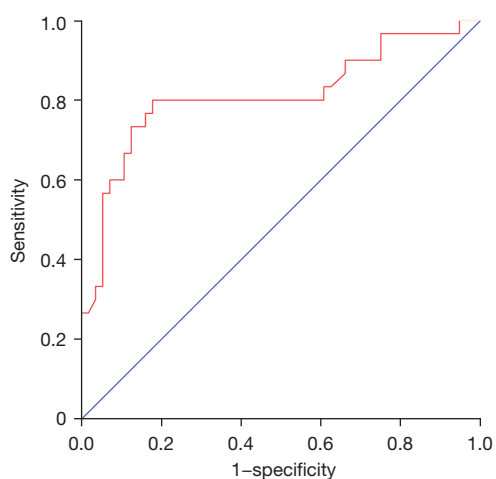
Figure 5 ROC analysis regarding the differentiation between high- and low-grade tumors using ΔPI%. ROC, receiver operating characteristic; ΔPI%, relative enhancement percentage index;

Association between MVD, angiogenesis differentiation, and WHO/ISUP grade

Our study found that both CD34- and CD31-identified MVD were lower in high-grade than in low-grade ccRCC tumors ($P<0.001$; *Figure 6A,6B*). The proportion of undifferentiated vessels (CD34⁻/CD31⁺) of high-grade tumors was significantly higher than that of low-grade tumors ($P<0.001$; *Figures 6C,7*). Undifferentiated vessels were negatively correlated with differentiated vessels (CD34⁺) (r=–0.248, P=0.021). This indicated that

the proliferation of undifferentiated vessels was often accompanied by a decrease in the number of differentiated vessels, and vice versa.

Association between CEUS features, MVD, and angiogenesis differentiation

The ΔPI% was positively correlated with MVD in both CD34 and CD31 staining (r=0.372, P<0.001 and r=0.315, P=0.003, respectively; *Figure 8A,8B*); however, it was negatively correlated with undifferentiated vessels (CD34⁻/CD31⁺) (r=–0.354, P=0.001). There was also a statistically significant difference in the density of undifferentiated vessels between the slow wash-in and fast wash-in cases ($P<0.001$).

Discussion

This retrospective study demonstrates that CEUS features can reliably differentiate between high- and low-grade ccRCC tumors. We found that a cut-off value of ΔPI% <33.15% (AUC =0.811) allowed for the identification of high-grade tumors. Moreover, MVD and ΔPI% were positively correlated, and there was a statistically significant difference in the density of undifferentiated vessels between the slow wash-in and fast wash-in cases. This suggests that the amount of contrast agent detected by CEUS is valid in representing tumor perfusion. Therefore, CEUS features could reliably evaluate tumor angiogenesis, MVD, and distinguish between undifferentiated vessels and
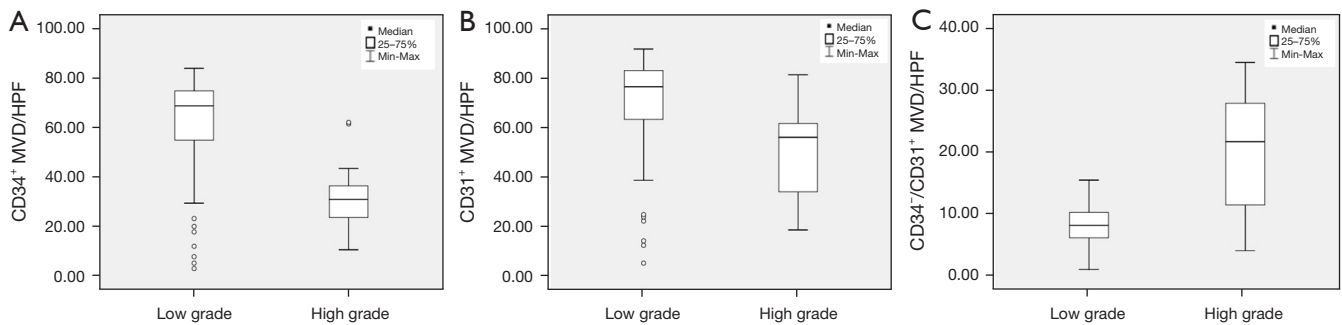
1888

Meng et al. Contrast-enhanced ultrasound for ccRCC

Figure 6 CD34⁺ MVD and CD31⁺ MVD were lower in high-grade than low-grade ccRCC (A,B), and undifferentiated vessels (CD34⁻/CD31⁺) were higher in high-grade than in low-grade ccRCC (C). (A) Association between MVD (CD34⁺ staining) and WHO/ISUP grade; (B) association between MVD (CD31⁺ staining) and WHO/ISUP grade; (C) association between MVD (CD34⁻/CD31⁺ staining) and WHO/ISUP grade. HPF, high power field; MVD, microvascular density; WHO/ISUP, World Health Organization/International Society of Urological Pathology.
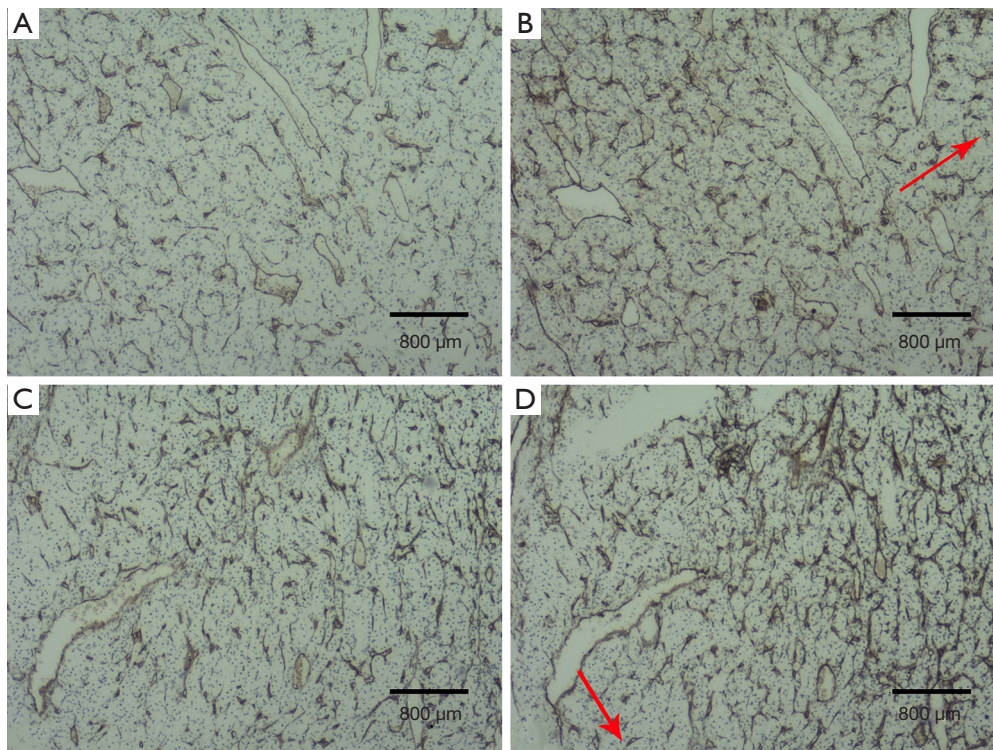

Figure 7 MVD of high- and low-grade ccRCC. (A) MVD (CD34⁺ staining) in high-grade tumors; (B) MVD (CD31⁺ staining) in high-grade tumors; (C) MVD (CD34⁺ staining) in low-grade tumors; (D) MVD (CD31⁺ staining) in low-grade tumors. The red arrows represent MVD (CD34⁻/CD31⁺ staining). Scale bar: 800 µm. ccRCC, clear cell renal clear cell carcinoma; MVD, microvascular density.

differentiated vessels.

The identification of tumor neovascularization is critical for optimizing the first-line selection of an appropriate treatment sequence for antiangiogenic therapy. In fact,

because different grades of ccRCC tumors differ in morphology and vasculature, their treatment methods and prognosis are different (17). Therefore, the nonsurgical evaluation of ccRCC grade is critical for the development
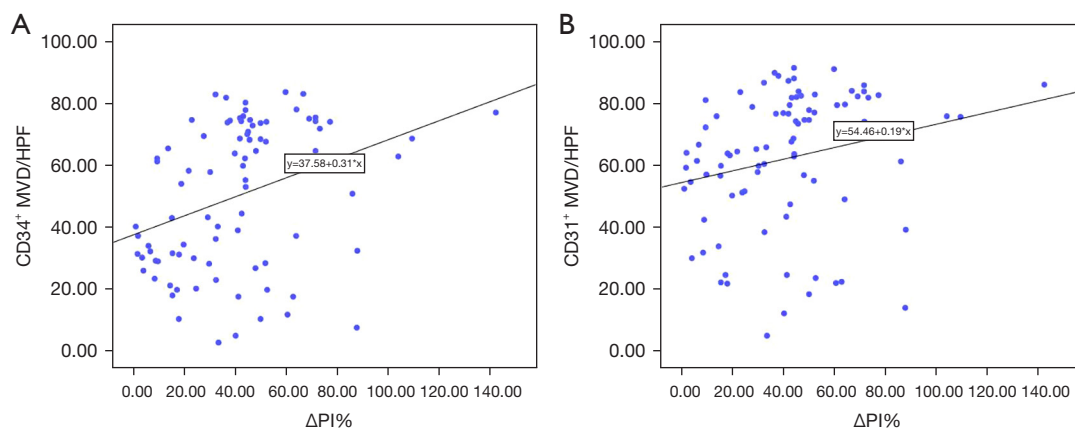
Figure 8 ΔPI% was positively correlated with CD34$^+$ MVD and CD31$^+$ MVD (A,B). (A) Association between ΔPI% and MVD (CD34$^+$ staining); (B) association between ΔPI% and MVD (CD31$^+$ staining). ΔPI%, relative enhancement percentage index; MVD, microvascular density; HPF, high power field.

of nonsurgical treatments. With regards to surgical examinations, renal tumor biopsy has been essential to evaluate the subtype and prognosis of RCC. However, the heterogeneity of RCC tumors sometimes makes it difficult to determine their subtype and grade (18). On the other hand, imaging methods may be more efficient, while also being less invasive than surgical procedures. For example, the diagnostic ability of multiphasic multidetector computed tomography (CT) on distinguishing ccRCC from other RCCs has been previously demonstrated. Pei *et al*. (19) showed that enhanced CT has high diagnostic efficiency for distinguishing between low- and high-grade ccRCC. Nonetheless, the use of this method and magnetic resonance imaging (MRI) is limited by radiation exposure, renal toxicity, and the presence of metal implants.

Multiple studies have focused on the nonsurgical evaluation of renal tumors with CEUS as a viable alternative to the aforementioned methods. The CEUS features of ccRCC and non-ccRCC have already been demonstrated to be significantly different (20), and PI has been described as a better parameter for representing enhancement. Furthermore, the ΔPI% index can help to avoid errors caused by individual differences across different patients (21). In this study, we successfully used the ΔPI% index to represent enhancement and distinguish between high- and low-grade tumors.

At present, the WHO/ISUP grading of ccRCC is the only tissue prognostic indicator included in RCC models. Measuring MVD is a method for both the quantitative evaluation of tumor neovascularization and the evaluation

of the degree of vascular differentiation (16). Some previous studies have reported that tumor grade is positively correlated with MVD (22-24), while others have stated that tumor grade is negatively correlated with MVD (25,26). These latter findings are consistent with our results.

The MVD is determined by vascular and non-vascular factors. When the metabolic level of tumor cells exceeds the level of angiogenesis, and the oxygen and nutrition supply to tumor cells is insufficient, tumor cell necrosis and MVD reduction occur. Although high-grade ccRCC still has some angiogenic activity, tumor cell necrosis, decreased MVD (27), increased capillary distance, and increased undifferentiated blood vessels in highly neovascularized areas are a result of the high metabolic state and severe hypoxia in tumoral tissues. Pericyte coverage is an important indicator of cell maturation (28), and the pericyte coverage of CD34$^+$ differentiated vessels is higher than that of CD34$^-$/CD31$^+$ undifferentiated vessels. These characteristics result in the specific morphology of undifferentiated vessels, which present as an absent or small lumen with a tortuous shape (9). This also explains the features of high-grade tumors that indicate a lack of blood supply, including lower MVD, more undifferentiated vessels, less edge enhancement, shorter duration of the contrast agent in the microvascular network, and slow wash-in. Some existing anti-vascular treatments have focused on reducing blood perfusion (29), while others have focused on reducing undifferentiated vessels and promoting vascular maturation (30). The outcome of both these methods can be evaluated nonsurgically through the abovementioned

CEUS features.

Despite our findings, our study still had certain limitations, including its retrospective nature, the small number of enrolled patients, and the variance in tumor grades assessed (most patients had either grade II or III tumors, while fewer had grade I or IV). In addition, to calculate the number of undifferentiated vessels, hotspots were chosen according to the most vascularized areas as assessed by CD31 staining intensity, so this may have ultimately resulted in a lower MVD value than that reported in other studies. Lastly, a certain degree of subjectivity in selecting the MVD hotspots and ROIs on the CEUS images cannot be completely excluded, although the selection criteria for determining both remained constant throughout the process.

Conclusions

In conclusion, the analysis of CEUS features can contribute to the nonsurgical diagnosis of ccRCC tumors, and our study has confirmed the reproducibility and high accuracy of CEUS to differentiate between low- and high-grade ccRCC. Future studies should be conducted in a prospective manner using a larger cohort to validate our results and assess whether incorporating CEUS features into clinical models will improve the ability of practitioners to predict high-grade tumors and optimize therapy for ccRCC patients.

Acknowledgments

Footnote

Conflicts of Interest: All authors have completed the ICMJE uniform disclosure form (available at https://dx.doi.org/10.21037/qims-21-291). The authors report that the research was supported by the Jilin Provincial Health Research Talents Special Project (20201231SY019).

Ethical Statement: The authors are accountable for all aspects of the work in ensuring that questions related to the accuracy or integrity of any part of the work are appropriately investigated and resolved. The study was conducted in accordance with the Declaration of Helsinki (as revised in 2013). The study was approved by the institutional Ethics Board of the China-Japan Union Hospital of Jilin University and all individual participants provided written informed consent.

References

1. Inamura K. Renal Cell Tumors: Understanding Their Molecular Pathological Epidemiology and the 2016 WHO Classification. Int J Mol Sci 2017;18:2195.

2. Leibovich BC, Lohse CM, Cheville JC, Zaid HB, Boorjian SA, Frank I, Thompson RH, Parker WP. Predicting Oncologic Outcomes in Renal Cell Carcinoma After Surgery. Eur Urol 2018;73:772-80.

3. Wang R, Hu Z, Shen X, Wang Q, Zhang L, Wang M, Feng Z, Chen F. Computed Tomography-Based Radiomics Model for Predicting the WHO/ISUP Grade of Clear Cell Renal Cell Carcinoma Preoperatively: A Multicenter Study. Front Oncol 2021;11:543854.

4. Vilaseca A, Guglielmetti G, Vertosick EA, Sjoberg DD, Grasso A, Benfante NE, Nguyen DP, Corradi RB, Coleman J, Russo P, Vickers AJ, Touijer KA. Value of Partial Nephrectomy for Renal Cortical Tumors of cT2 or Greater Stage: A Risk-benefit Analysis of Renal Function Preservation Versus Increased Postoperative Morbidity. Eur Urol Oncol 2020;3:365-71.

5. Fang T, Xiao J, Zhang Y, Hu H, Zhu Y, Cheng Y. Combined with interventional therapy, immunotherapy can create a new outlook for tumor treatment. Quant Imaging Med Surg 2021;11:2837-60.

6. Delahunt B, Eble JN, Egevad L, Samaratunga H. Grading of renal cell carcinoma. Histopathology 2019;74:4-17.

7. Folkman J. Tumor angiogenesis. Adv Cancer Res 1985;43:175-203.

8. Jilaveanu LB, Puligandla M, Weiss SA, Wang XV, Zito C, Flaherty KT, Boeke M, Neumeister V, Camp RL, Adeniran A, Pins M, Manola J, DiPaola RS, Haas NB,

Kluger HM. Tumor Microvessel Density as a Prognostic Marker in High-Risk Renal Cell Carcinoma Patients Treated on ECOG-ACRIN E2805. Clin Cancer Res 2018;24:217-23.

9. Qian CN, Huang D, Wondergem B, Teh BT. Complexity of tumor vasculature in clear cell renal cell carcinoma. Cancer 2009;115:2282-9.

10. Lima A, van Rooij T, Ergin B, Sorelli M, Ince Y, Specht PAC, Mik EG, Bocchi L, Kooiman K, de Jong N, Ince C. Dynamic Contrast-Enhanced Ultrasound Identifies Microcirculatory Alterations in Sepsis-Induced Acute Kidney Injury. Crit Care Med 2018;46:1284-92.

11. Eso Y, Nakano S, Mishima M, Arasawa S, Iguchi E, Takeda H, Takai A, Takahashi K, Seno H. A simplified method to quantitatively predict the effect of lenvatinib on hepatocellular carcinoma using contrast-enhanced ultrasound with perfluorobutane microbubbles. Quant Imaging Med Surg 2021;11:2766-74.

12. Mueller-Peltzer K, Negrao de Figueiredo G, Graf T, Rübenthaler J, Clevert DA. Papillary renal cell carcinoma in contrast-enhanced ultrasound (CEUS) - A diagnostic performance study. Clin Hemorheol Microcirc 2019;71:159-64.

13. Wei S, Tian F, Xia Q, Huang P, Zhang Y, Xia Z, Wu M, Yang B. Contrast-enhanced ultrasound findings of adult renal cell carcinoma associated with Xp11.2 translocation/TFE3 gene fusion: comparison with clear cell renal cell carcinoma and papillary renal cell carcinoma. Cancer Imaging 2019;20:1.

14. King KG, Gulati M, Malhi H, Hwang D, Gill IS, Cheng PM, Grant EG, Duddalwar VA. Quantitative assessment of solid renal masses by contrast-enhanced ultrasound with time-intensity curves: how we do it. Abdom Imaging 2015;40:2461-71.

15. Weidner N, Semple JP, Welch WR, Folkman J. Tumor angiogenesis and metastasis--correlation in invasive breast carcinoma. N Engl J Med 1991;324:1-8.

16. Yao X, Qian CN, Zhang ZF, Tan MH, Kort EJ, Yang XJ, Resau JH, Teh BT. Two distinct types of blood vessels in clear cell renal cell carcinoma have contrasting prognostic implications. Clin Cancer Res 2007;13:161-9.

17. Escudier B. Combination Therapy as First-Line Treatment in Metastatic Renal-Cell Carcinoma. N Engl J Med 2019;380:1176-8.

18. Warren AY, Harrison D. WHO/ISUP classification, grading and pathological staging of renal cell carcinoma: standards and controversies. World J Urol 2018;36:1913-26.

19. Pei X, Wang P, Ren JL, Yin XP, Ma LY, Wang Y, Ma X, Gao BL. Comparison of Different Machine Models Based on Contrast-Enhanced Computed Tomography Radiomic Features to Differentiate High From Low Grade Clear Cell Renal Cell Carcinomas. Front Oncol 2021;11:659969.

20. Kasoji SK, Chang EH, Mullin LB, Chong WK, Rathmell WK, Dayton PA. A Pilot Clinical Study in Characterization of Malignant Renal-cell Carcinoma Subtype with Contrast-enhanced Ultrasound. Ultrason Imaging 2017;39:126-36.

21. Sun D, Wei C, Li Y, Lu Q, Zhang W, Hu B. Contrast-Enhanced Ultrasonography with Quantitative Analysis allows Differentiation of Renal Tumor Histotypes. Sci Rep 2016;6:35081.

22. Fan C, Zhang J, Liu Z, He M, Kang T, Du T, Song Y, Fan Y, Xu J. Prognostic role of microvessel density in patients with glioma. Medicine (Baltimore) 2019;98:e14695.

23. Ebru T, Fulya OP, Hakan A, Vuslat YC, Necdet S, Nuray C, Filiz O. Analysis of various potential prognostic markers and survival data in clear cell renal cell carcinoma. Int Braz J Urol 2017;43:440-54.

24. Tu J, Ying X, Zhang D, Weng Q, Mao W, Chen L, Wu X, Tu C, Ji J, Huang Y. High expression of angiogenic factor AGGF1 is an independent prognostic factor for hepatocellular carcinoma. Oncotarget 2017;8:111623-30.

25. Cioca A, Muntean D, Bungardean C. CD105 as a tool for assessing microvessel density in renal cell carcinoma. Indian J Pathol Microbiol 2019;62:239-43.

26. Nakanishi H, Miyata Y, Mochizuki Y, Yasuda T, Nakamura Y, Araki K, Sagara Y, Matsuo T, Ohba K, Sakai H. Pathological significance and prognostic roles of densities of CD57+ cells, CD68+ cells, and mast cells, and their ratios in clear cell renal cell carcinoma. Hum Pathol 2018;79:102-8.

27. Hlatky L, Hahnfeldt P, Folkman J. Clinical application of antiangiogenic therapy: microvessel density, what it does and doesn't tell us. J Natl Cancer Inst 2002;94:883-93.

28. Thijssen VL, Paulis YW, Nowak-Sliwinska P, Deumelandt KL, Hosaka K, Soetekouw PM, Cimpean AM, Raica M, Pauwels P, van den Oord JJ, Tjan-Heijnen VC, Hendrix MJ, Heldin CH, Cao Y, Griffioen AW. Targeting PDGF-mediated recruitment of pericytes blocks vascular mimicry and tumor growth. J Pathol 2018;246:447-58.

29. Tamma R, Rutigliano M, Lucarelli G, Annese T, Ruggieri S, Cascardi E, Napoli A, Battaglia M, Ribatti

1892

Meng et al. Contrast-enhanced ultrasound for ccRCC

D. Microvascular density, macrophages, and mast cells in human clear cell renal carcinoma with and without bevacizumab treatment. Urol Oncol 2019;37:355.e11-9.

30. Rizov M, Andreeva P, Dimova I. Molecular regulation and role of angiogenesis in reproduction. Taiwan J Obstet Gynecol 2017;56:127-32.